EXPERIMENTAL AND THEORETICAL INVESTIGATION OF AN UNUSUALLY SHAPED HORN

J Panzer R&D TEAM, Salgen, Germany
P Macey PACSYS, Nottingham, UK

This paper reports on the investigation of the sound pressure response and radiation impedance of a loudspeaker horn driven by an electro-dynamic transducer. The investigation has three parts, the measurement and further the simulation using two independent programs, using finite and boundary element methods. Issues associated with meshing for the BEM and FEM and the experimental setup are discussed.

1 INTRODUCTION

In this paper we present the modeling of the frequency response of a given horn. Our curiosity is focused on the results of the simulation software applications used and how the results would compare. Also presented is the measured directivity, which provides a further point of comparison.
The simulation tools used solve the wave-equation in the frequency domain for given boundary conditions. As a result we can obtain observations of the sound pressure response and the radiation impedance.
To understand the performance of the horn, independent of its environment, and without any contribution from diffraction of baffle edges and room acoustic effects, it is informative to study its performance when it is mounted in an infinite rigid baffle and radiating into a half space.
For comparison of the calculation results we selected two quantities. Firstly, the lumped acoustic radiation impedance at the throat of the waveguide. Secondly, the sound pressure level at a certain fixed distance at various angles in front of the baffle.
The lumped acoustic radiation impedance is notoriously difficult to measure. However, it is straightforward to extract from a simulation model. The radiation impedance is an important parameter for the design of a waveguide because the radiated power is proportional the radiation resistance. Further, its curves are ideal candidates when it comes to compare the results of simulation software. This is so because the calculation of the lumped radiation impedance involves the whole acoustic field as an integral value.
The reason, why we selected the sound pressure is that it is easily reproduced by calculation, and also because we have had available the measurement device for taking directivity sound pressure measurements.

2 THE WAVEGUIDE

The device under test is a little horn or waveguide of over-all dimensions:

Mouth width x height	95 x 95 mm
Throat diameter	12.7 mm
Length	170 mm

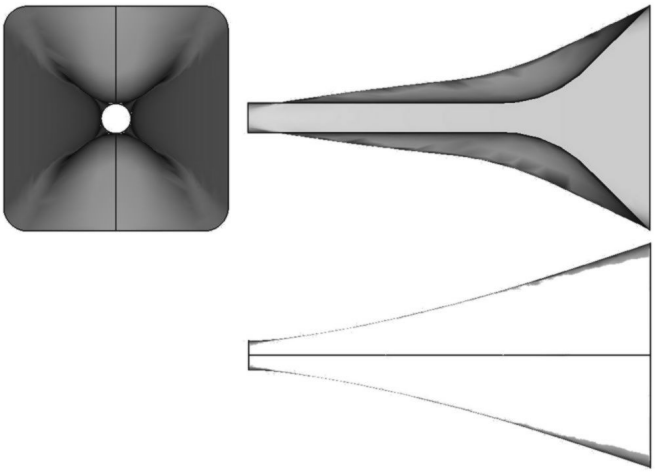

Figure 1: Sketch of waveguide

Figure 1 shows a sketch of the view into the mouth, a cut of the view of the curved sides and a cut of the view of the linear sides.
The flair of the horn does not follow any particular mathematical function. It has been designed with the help of a CAD-tool. Basically the waveguide opens linearly with a slight curvature in the first quarter along the horn. Additionally there is a bump on two opposite sides yielding a constriction along the center of the horn.

3 LUMPED ACOUSTIC RADIATION IMPEDANCE

During development of a waveguide for a loudspeaker the designer typically has a close look at the curve of the lumped acoustic radiation impedance. This is so because the acoustic output power of the horn is proportional to the real part of this impedance. Hence, the variations of the impedance curve will inevitably have an effect on the sound quality of the speaker. When we speak here of the radiation impedance we mean the lumped acoustic impedance of the piston mode at the throat:

$$Z_a = \frac{p}{q} \tag{1}$$

with volume velocity $q = v \cdot S_{th}$ and sound pressure p. We assume here that the acoustic velocity v is constant (pistonic) over the cross-sectional area of the throat S_{th} and points into the same direction. In formula 1 the sound pressure is thought to be a mean value over S_{th}. A plausible mean-value can be obtained with the help of the acoustic power, which is in general:

$$P_a = \frac{1}{2} \cdot \int_S p \cdot \vec{\hat{v}} \, d\vec{S} \tag{2}$$

here, the factor "½" comes from the crest-factor of a sinusoidal wave where we assume p and v to be peak values of a sinuidal signal. The acoustic velocity is a vector and we take the conjugate complex value. S can be any area. Then P_a is the acoustic power through that area.
If we combine formula 1 and formula 2 under the assumptions of uniform velocity (pistonic, v = 1) and S being the cross-section at the throat then this would yield for the radiation impedance:

$$Z_a = \frac{1}{S_{th}^{\,2}} \cdot \int_{S_{th}} p \, dS \tag{3}$$

hence, the lumped radiation impedance at the throat would be proportional to the mean-value of the pressure, if the horn is excited by a uniform acoustic velocity. This condition can be easily satisfied inside a simulation algorithm. However, for a measurement the uniform velocity condition would be

more difficult to achieve, especially at frequencies where the wavelength is small compared to the dimension of the throat.
Having available the impedance Z_a one can calculate the acoustic power of the piston mode of the horn. Its real part is proportional to the acoustic power radiated into the far-field:

$$P_a = \frac{1}{2} \cdot Z_a \cdot |v|^2 \cdot S^2 \tag{4}$$

One can show that the lumped acoustic radiation impedance approaches always a certain value asymptotically at high frequencies, which is

$$Z_{ao} = \frac{\rho c}{S_{th}} \tag{5}$$

Formula 5 can be used to normalize the radiation impedance, so that the real part of any curve would approach the value of one at high frequencies. The imaginary goes to zero.

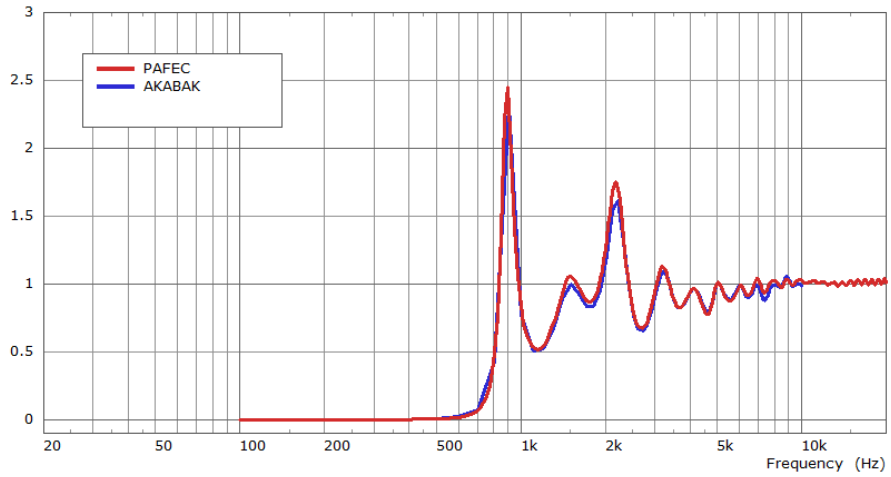

Figure 2: Calculated normalized lumped radiation resistance at the throat of example horn as shown in figure 1.
PAFEC red and AKABAK blue.

Figure 2 shows the result of the calculation of formula 3. Displayed is the real part of the normalized lumped radiation impedance at the throat of the horn if excited by uniform driving velocity (piston-mode). The normalization is done by applying formula 5, hence the curves should approach the value of one at high frequencies. The curves of Figure 2 can be regarded as a transmission characteristic and, hence, have a high-pass character. The stop-band is at low frequencies below approximately 500 Hz. At high frequencies the radiated power will follow the spectrum curve of the velocity at the throat. Between 500 Hz and 3 kHz the horn radiates selectively. For example at 900 Hz the radiated sound power would be more than twice than at high frequencies. At 1.2 kHz the transmission is strongly attenuated. These fluctuations could be altered by changing the horn geometry.
In this paper we want to draw the attention to the fact that there are two curves which are almost identical. The red curve is the result of the PAFEC-simulator whereas the blue curve results from the AKABAK-simulator. These two software tools calculate the same response of the device under test. Their results are almost identical although the internal working of these software tools is different.

4 MEASUREMENT

For the measurement of the directivity the horn is driven by a compression driver. The exit of its phase plug has a diameter of 12.7 mm which fits perfectly to the throat diameter of the waveguide.

In this paper we focus on the normalized directivity. The normalization hides the influence of the properties of the driver. Hence, there is no need to describe the compression driver in detail. The response is linear because adjusting the drive voltage did not affect the directivity pattern.

Figure 3: Directivity measurement set-up

The horn is fitted into a rotatable baffle of size 910 x 600 mm as shown in figure 3. The directivity is the sound pressure in the far-field at various position of equal distance between the microphone and the center of the mouth. The distance of the microphone is d = 700 mm. The baffle is rotated in the horizontal plane in 5 deg steps. The other dimension of rotation comes from a rotation about the on-axis. In this way a whole so-called balloon directivity measurement could be performed. However, in this paper we regard only the polar measurement of the horizontal plane (azimuth = 0 deg) and of the vertical plane (azimuth = 90 deg).

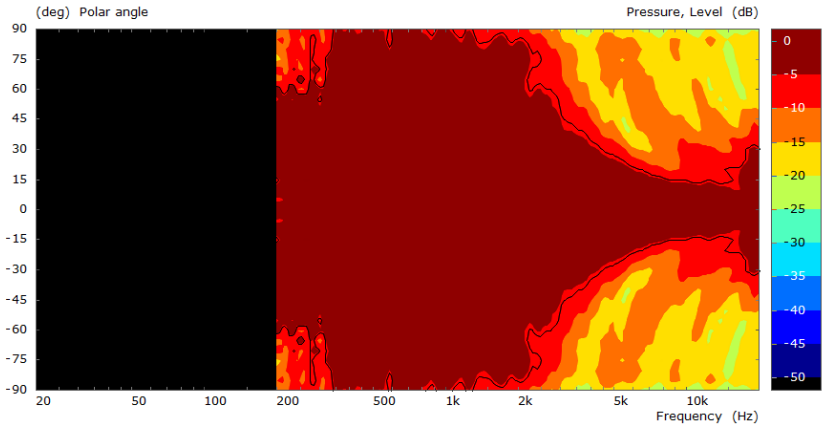

Figure 4: Frequency-directivity contour plot of example horn in the horizontal plane (linear walls)

Figure 4 displays the measurement of normalized sound pressure level taken at 19 microphone positions in a regular angular range between 0 deg to 90 deg. The map is mirrored to display the whole range from -90 deg to 90 deg. The colored contours range from -50 dB to 0 dB. For normalization each spectrum of the sound pressure is divided by the spectrum in on-axis direction (0 deg). The fine outline displays the contour at -6dB which is also called the beamwidth curve. At low frequencies the horn should radiated almost omni-directional. The slight deviations are caused by diffraction of the finite baffle and other insufficiency of the measurement situation.

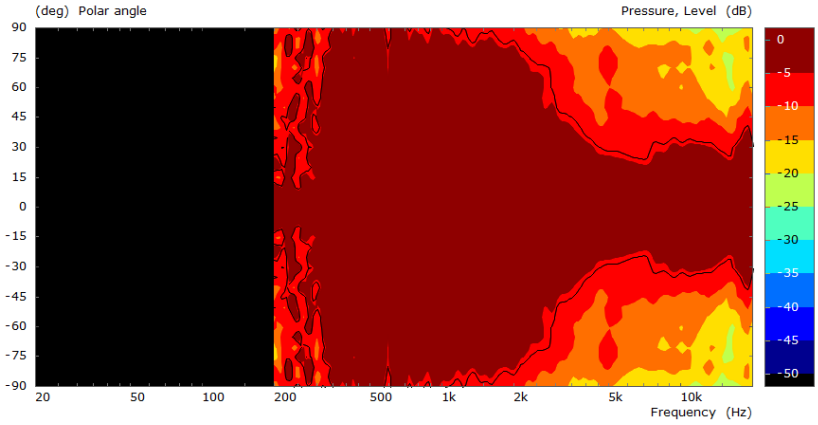

Figure 5: Frequency-directivity contour plot of example horn in the vertical plane (curved walls)

Figure 5 shows the directivity in the vertical plane. In comparing the plot to the one of figure 4 it is obvious that the beamwidth is broader. This is likely caused by the smaller aperture due to the bumps inside the horn.

4.1 Comparison of Directivity Calculations

Both simulation applications are able to calculate the sound pressure at the same locations as used for the measurement. The virtual microphone is placed at constant distance d = 700 mm from the center of the horn mouth. Starting at the on-axis direction calculations are done at various angles in the horizontal and vertical planes. The angular distance between the positions is 5 deg.

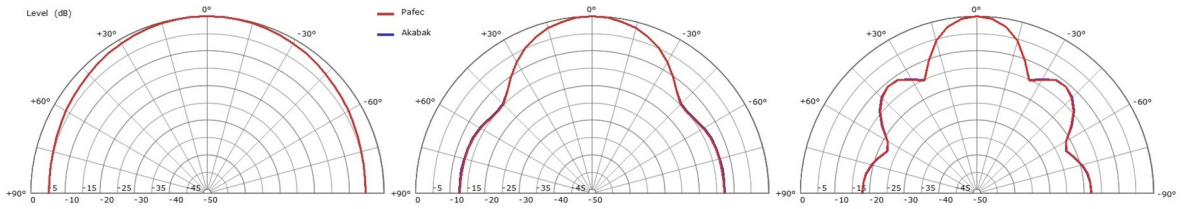

Figure 6: Directivity in horizontal plane (linear walls)
PAFEC red and AKABAK blue
at frequencies 2k Hz, 5 kHz, 8 kHz

Figure 5 shows the angular distribution of the sound pressure level in the horizontal plane. The polar-plot shows curves at 2 kHz, 5 kHz and 8 kHz. At 2 kHz the horn radiates almost omni-directional. At 5 kHz beam-forming starts. At 8 kHz radiation to the side is attenuated and most energy is radiated on-axis. The red curve is the result of the PAFEC-simulator and the blue curve is the result of the AKABAK-simulator. The plot demonstrates the similarity of the calculation results.

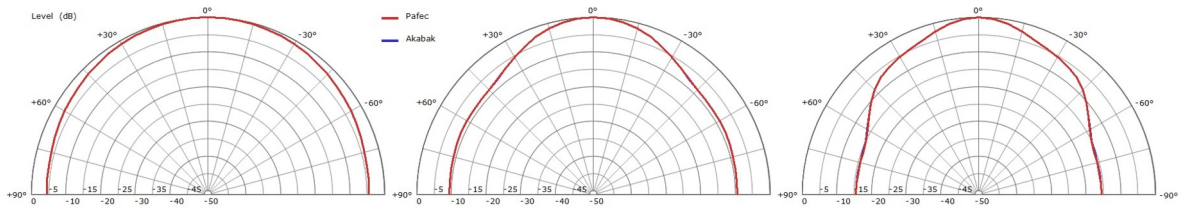

Figure 7: Directivity in horizontal plane (curved walls)
PAFEC red and AKABAK blue
at frequencies 2k Hz, 5 kHz, 8 kHz

Figure 5 shows the overlay of the simulated curves in the vertical plane. The broader pattern is caused by the bump which yields a constricted aperture.

4.2 Comparison of Measurement and Simulation

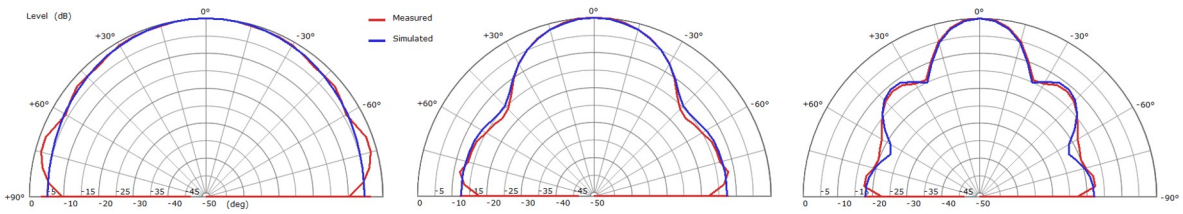

Figure 8: Directivity in horizontal plane (linear walls)
measured versus simulated
at frequencies 2k Hz, 5 kHz, 8 kHz

Figure 8 demonstrates an overlay of simulated and measured directivity curves in the horizontal plane which curves are predominantly caused of the linear walls of the horn.

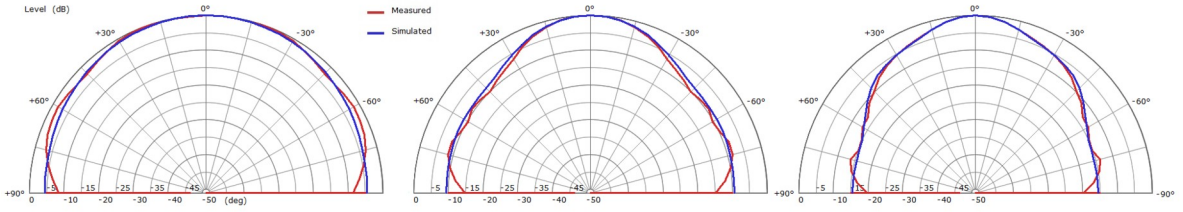

Figure 9: Directivity in horizontal plane (curved walls)
measured versus simulated
at frequencies 2k Hz, 5 kHz, 8 kHz

Figure 9 shows an overlay of simulated and measured curves in the vertical plane.
There is a good agreement between the simulated and the measured results. The deviations close to 90 deg are due to the fact that for the measurement the infinite baffle is finite after all.

5 MODELING FOR SIMULATION

The horn is mounted with its mouth flush in an infinite baffle. The infinite baffle is reflecting and its boundary condition means that the component of the acoustic velocity which is normal to its plane should be zero everywhere. The Sommerfeld radiation condition must be satisfied, to ensure that the pressure field in the half space consists of outgoing waves.

5.1 Simulation Methods and Subdomain Modelling

Many simulation methods are used in acoustics including finite difference, finite volume, finite element (FEM) and boundary element (BEM). In the current work FEM and BEM simulations are used. Each of these methods has strengths and weaknesses and it is consequently sometimes beneficial to split the acoustic domain into subdomains.

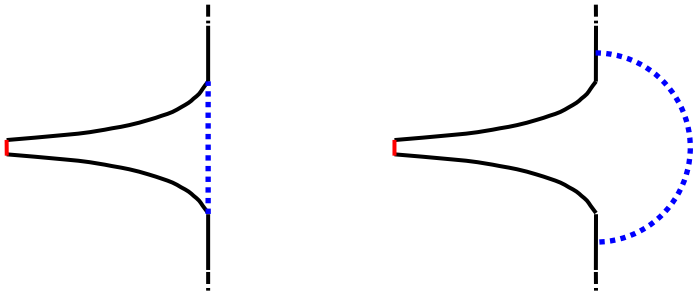

Figure 10: Subdomain modelling.
Left: Splitting at mouth of horn.
Right: Splitting at hemispherical surface

Two such decompositions are shown in figure 10. Finite difference and finite volume approaches are obtained directly from the Helmholtz equation, using differencing operations to approximate derivatives. The finite element method is also closely related to the underlying differential equation, which is multiplied by a weighting function and integrated by parts. The domain is decomposed into small elements such that the pressure can be assumed to vary as a linear combination of some suitable basis functions, e. g. low order polynomials, within each element. Applying the Galerkin method produces the FEM linear equations. The boundary element method attempts to solve a derived integral equation, using a set of local basis functions on the bounding surface of the acoustic volume; within the domain itself the solution of the Helmholtz equation is ensured by the properties of the Green's function. Only FEM and BEM are considered further, as they are used for the results in this study, see also for example [4] and [5]. Both methods produce a set of linear equations which are solved to determine the pressure at the nodes in the model. For FEM a large set of sparse equations are produced, as nodes are required on elements throughout the volume. For BEM a smaller dense set of equations is produced from the nodes on the surface elements. In both cases the element size has to be small enough to adequately represent the pressure variation, which in turn is usually related to the acoustic wavelength. Analysis at higher frequencies requires smaller elements, more nodes and hence has greater computational requirements: CPU time, memory and disk space.
The surface of the horn has a sharp fold, particularly near the throat, such that the radius of curvature is smaller than the element side-length which is needed from frequency-based considerations. There is hence a concern that the geometry may not be adequately represented. This can be checked using mesh convergence.
The geometry and boundary conditions of the idealized problem have two planes of symmetry. It is thus possible to reduce the problem size by using a quarter model. All the simulations in this paper were using quarter models.

5.2 AKABAK

The AKABAK simulator [1] calculates the acoustic field inside the horn and in front of the baffle with the help of the boundary element method. The calculation of the Helmholtz Integral is usually a two stage process. Firstly, one has to solve for certain unknown parameters of the integral. If available, one can commence with the calculation of the observation points. In order to solve for the unknown parameters one divides the surface of the acoustic boundary into small elements. Typically, the mesh-density needs to be found experimentally, one only knows that the result becomes exact with infinitely small elements. Otherwise we get an approximation. Because only surface values of pressure and velocity are to be integrated, the mesh need to be of two dimensions only [3].

5.3 Subdomain Modelling

There exists a special Green-function which satisfies automatically the condition of zero normal velocity on the infinite baffle plane. Hence, there is no need to mesh this boundary. However, this function would be valid only for boundary elements which are in or in front of the baffle.

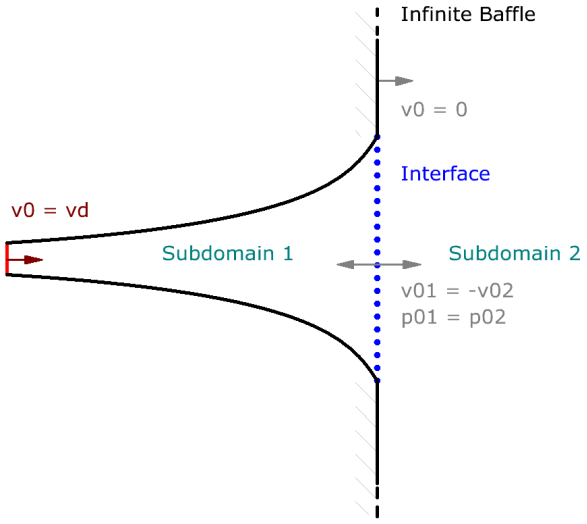

Figure 11: Subdomain modeling

If there are acoustic boundaries behind the infinite baffle the calculation of the acoustic field becomes more complicated. As our horn ends in the plane of the baffle all walls of the horn are behind the infinite baffle. The trick to be applied consists of dividing the radiation domain into two subdomains as sketched in figure 11. In-between one creates an interface where at any point there is guarantied a continuity of parameters. The interface is acoustically transparent. On its surface the pressure of subdomain 1 is equal to the surface pressure of subdomain 2. Likewise, should the acoustic velocity be equal. Here we consider the velocity-component normal to the plane of the interface. The negative sign comes in because one regards the vectors pointing into the subdomain.

5.4 Driving

The specified boundary condition is concerned only with the surface velocity. The reflecting boundaries feature a zero normal velocity. However, the cross-section at the throat of the horn has an imprinted velocity. This motion is specified here to be uniformly distributed and simply of value one, as labeled in figure 11 by velocity v_d. The surface pressure is the parameter of solving.

5.5 Meshing

The geometry of the acoustic boundary is meshed with the help of GMSH [3], which is an external meshing tool specialized for producing elements for the boundary and finite element analysis. Only a 2D-mesh needs to be produced as we consider only the surface. The imported mesh is then refined by AKABAK to make sure all elements are smaller than a specified edge length. For the shown simulation a mesh of 1906 triangles was used for the boundaries of the horn and 1040 for the interface. We assume a constant pressure over each element. Experimentation of varying the mesh-density showed that results could be regarded sufficiently accurate up to a frequency of 10 kHz.

5.6 PAFEC

Two modeling strategies were employed to analyze the baffled horn in PAFEC VibroAcoustics [2]. In the first approach the subdomain splitting of figure 10-left was used with 10-noded quadratic tetrahedral acoustic finite elements used in subdomain 1 and a Rayleigh integral boundary element composed of 6-noded quadratic triangles. The model BEM1 had 55096 acoustic finite element degrees of freedom and 2453 acoustic boundary element degrees of freedom. Based on a criterion of 3 quadratic elements/wavelength should be valid up to 20 kHz, however because of the small radius of curvature on the "fold", the size of elements may perhaps not have adequately represented the geometry. In many situations, where there is not constricted geometry, deviations by distances small compared with the acoustic wavelength should not significantly affect the results. To confirm this, a finer mesh density model BEM2 was run. This had 339045 acoustic finite element degrees of freedom and 9212 boundary element degrees of freedom, should be valid to 40 kHz and was much closer the geometry in the problematic area of the sharp fold near to the throat.

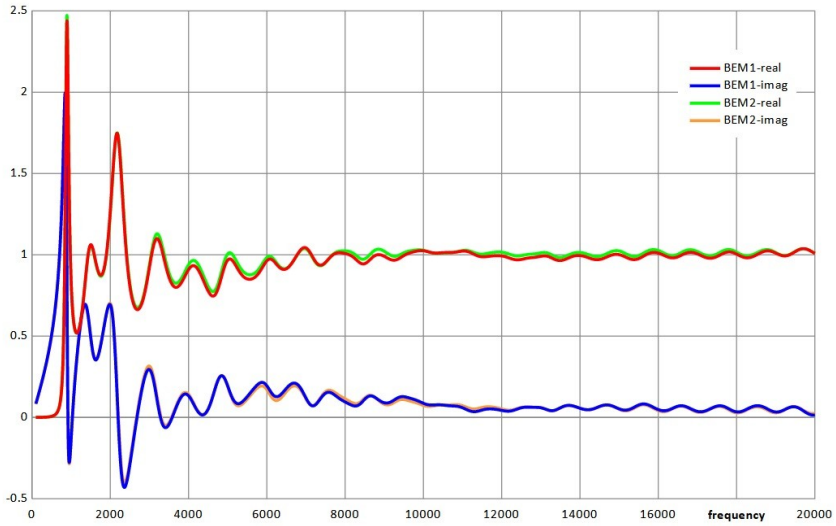

Figure 12: Throat impedance computed by method BEM1 & BEM2

Figure 12 compares the throat impedance for the two models. The agreement is good. BEM2 is used as a reference standard below in figure 14.

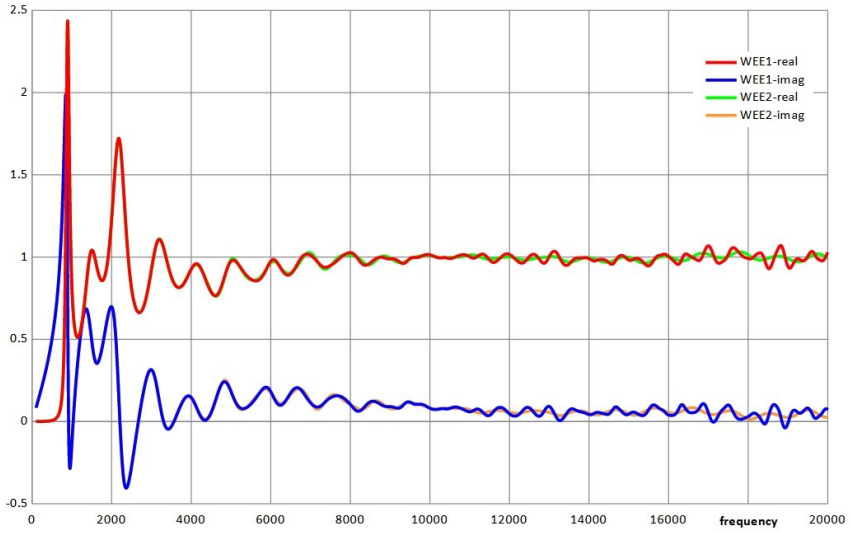

Figure 13: Throat impedance computed by WEE1 & WEE2

In the second approach the subdomain splitting was as in figure 10-right. Acoustic finite elements were used in subdomain 1 extending from the throat to a hemispherical surface and wave envelope elements were used in subdomain 2 for the remainder of the half space. Wave envelope elements are similar to finite elements but extend out to infinity. The basis functions are outward traveling waves, monopole, dipole, etc. A wave envelope element based approach can be faster than a BEM-based approach, but the accuracy is affected by the radius of the spherical surface at the interface between the subdomains and the number of terms used for outward traveling waves (= radial order). Model WEE1 had the hemispherical surface extending out to 0.072 m and had radial order 2 and a total of 173915 acoustic degrees of freedom. Model WEE2 had a hemispherical radius of 0.102 m, radial order 6 and a total of 229368 acoustic degrees of freedom. Both meshes were valid to 20 kHz, based on the 3 quadratic elements/wavelength criterion. Figure 13 compares throat impedances for WEE1 & WEE2.

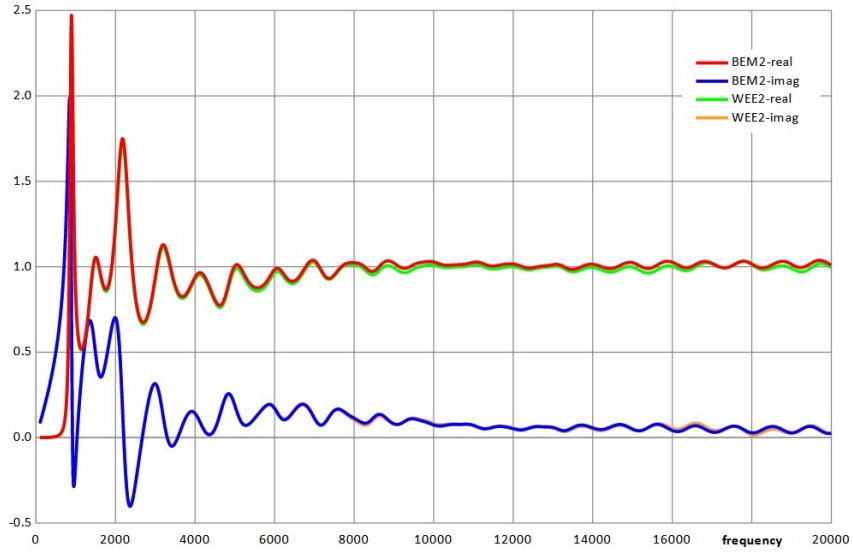

Figure 14: Throat impedance computed by BEM2 & WEE2

Figure 14 compares the models BEM2 & WEE2. The model WEE1 becomes less accurate at higher frequencies. It is concluded that a wave envelope element approach can produce accurate results up to high frequency, but it is necessary to take care with the hemispherical radius and radial order.

6 FURTHER WORK

We would like to extend the work to model the electro-dynamic compression driver so we can compare absolute sound pressure values of measurement and simulation. In that scenario AKABAK would model the compression driver with the help of the lumped element method whereas PAFEC would use the finite element method as a modeling algorithm.

7 ACKNOWLEDGEMENT

The second author gratefully acknowledges the assistance of his colleague John King by doing some of the model preparation work.

8 REFERENCES

1. AKABAK, software simulation tool, www.randteam.de.
2. PAFEC level 8.8, Acoustics manual, Strelley Hall, Nottingham, NG8 6PE, UK, on request.
3. GMSH, software for 2D and 3D meshing, www.gmsh.info.
4. Atalla N, Sgard F: *Finite Element and Boundary Methods in Structural Acoustics and Vibration*; CRC Press, 2017.
5. Marburg S, and Nolte B: *Computational Acoustics of Noise Propagation in Fluids: Finite and Boundary Element Methods,* Springer 2008.